https://doi.org/10.5194/angeo-2021-34
Preprint. Discussion started: 23 June 2021


Annales Geophysicae Discussions
Open Access

# Latitude Oscillations of Zonal Mean Total Electron Content and Super-Fountain Effects Provided from Global GNSS Stations

**Mohammad Joghataei[1],** Niloofar **Jooyandeh[1] and Mohammad Hossein Memarian[1]**

1- Department of Physics, Yazd University, Yazd, Iran

Corresponding author: Mohammad Joghataei (mjoghataei@yazd.ac.ir)

**Key Points:**

- The zonal mean GPS-TEC can detect the behaver of equatorial ionosphere anomaly as well as super-fountain effect
- Latitude variations of zonal means of TEC exhibit higher maximum values or TEC in NH spring equinox than fall equinox
- Upward propagating planetary waves induce fluctuations on zonal mean TEC of mid-latitude

https://doi.org/10.5194/angeo-2021-34
Preprint. Discussion started: 23 June 2021


Annales Geophysicae Discussions


**Abstract**

Seasonal and latitude oscillations of equatorial ionization anomaly (EIA) were investigated by zonal mean total electron content (TEC) provided from global gridded GNSS data from 1999 to 2017. Maximum monthly zonal mean TEC values showed NH spring equinox's value is higher than fall's. Some fluctuations are observed due to upward planetary wave propagation in equinoxes and winter especially in low solar activity. Two cases of super-fountain effect were also clearly detected on zonal mean TEC.


## 1 Introduction

Equatorial ionization anomaly (EIA) is one of the interesting phenomena in low-latitude ionosphere, which is also known as Appleton anomaly and fountain effect (*Appleton*, 1946). Plasma density on both sides of the magnetic equator is raised as a consequence of E×B upward plasma drifts which lifts the plasma from magnetic equator to higher altitudes. The lifted plasma diffuses down along magnetic field to the higher latitude due to the gravitational and the plasma pressure gradient forces. As a consequence, ionization enhancements on both sides of the magnetic equator, forming the structure with two ionization crests near ±15° geomagnetic latitudes and a trough at geomagnetic equator. At dusk, when the eastward winds are the strongest, a strong vertical drift is produced that is called "pre-reversal enhancement" of the zonal electric field. An interhemispheric wind blowing from the summer to the winter hemispheres produces an asymmetry between crests' density (*Abdu et al.,* 2003). Monthly-hourly EIA oscillations and monthly EIA crests contain different interesting aspects such as variable thermospheric winds, conductivity distributions, which have not been fully understood. Although studies about longitude variations, annual, semiannual, seasonal of EIA have already been conducted (*Fejer et al.*, 2008; *Mo et al.*, 2018; *Wu et al.*, 2004), its latitude interconnection can also help to understand other aspects of the problem.

Longitudinal variations of EIA may be due to some effects such as: difference in magnetic declination, E×B drift, stationary and tidal waves and neutral winds in different longitudes (*Fejer et al.*, 2008; *Lin et al.*, 2007). *Tsai et al.* (2001) have reported greater total electron content (TEC) values in the southern/winter hemisphere during July and August 1997, and also indicated that the EIA crests in the winter hemisphere formed earlier than that in the summer hemisphere. *Scherliess and Fejer* (1999) showed that equatorial upward E×B drift reaches its maximum value between 10:00 to 11:00 LT and hence more noticeable plasma transportation occurs after that time as fountain effect. The maximum diurnal of TEC location, and therefore the EIA crest vary with the season and the solar activity in that EIA are stronger and somewhat higher latitude in equinox months than that in solstice months, and also in the solar maximum years than the solar minimum years (*Lin et al.*, 2007). However, the precise amount of maximum values and locations of zonal mean TEC and latitudinal variation of EIA were not well established.
The equatorial electrojet (EEJ), that is driven by the Pedersen east-west electric field in the lower E region, has significant effects on EIA. E×B drift results in a downwards Hall current, supporting vertical charge separation across the ionosphere. This effect in turns gives an upwards secondary electric field and a secondary Pedersen current opposite to the primary Hall current. The secondary Hall current also reinforces the original Pedersen current. As electric field get strength then upward drift of plasma changes in the amount of plasma raised that diffuses downward to low latitudes

https://doi.org/10.5194/angeo-2021-34
Preprint. Discussion started: 23 June 2021



along the magnetic field lines (*Bhuyan and Bhuyan*, 2009). The diurnal, seasonal, and solar cycle variations of EIA crest is consistent with the strength of EEJ (*Mo et al.*, 2018). The diurnal variation of the EIA location with EEJ strength should be better than the EIA crest TEC with EEJ strength (*Mo et al.*, 2018). On the other hand, the semiannual variation of TEC is more pronounced in the equatorial regions due to the interaction of solar zenith angle and atmospheric circulation over the high-latitude regions which result in changing amount of oxygen to nitrogen ratio (*Fuller*, 1998). In conclusion, due to the complex spatiotemporal nature of EIA, climatology of TEC can better clarify different aspects of EIA and also latitude variations show some new insights into nature of the problem.

An accepted approach to diagnose spatiotemporal structure of ionospheric variability is application of TEC (*Saito et al.*, 1998). TEC is the number of electrons in a column of one square meter cross section that extends from the ground up to topside ionosphere. In recent years, two frequencies of the GPS signals have been widely used for estimation and modeling regional and global TEC values (*Liao 2000; Gao and Liu, 2002*). Some advantages of GNSS data are the large number of GPS satellites, their global coverage and the availability of commercial receivers. For this purpose, first standard RINEX format was released in September and October 1990 (*Schaer et al., 1998*). By using programs and models to process RINEX data, ionospheric delays are calculated and therefore values of electron content are obtained. The format of the produced data in this manner is IONEX. The global gridded IONEX products support 2- and 3-dimentional TEC maps (*Schaer et al.,1998*). Here climate features of EIA will be considered with IONEX data. However, in this paper, we are focusing on any latitudinal interconnections of zonal mean TEC.

This paper is organized as follows. The second section examines IONEX and F10.7 data, in which horizontal and temporal resolution of data are described in details. In addition, the methodology of calculation of means and classification of data is described. Then the results of TEC data are presented with specific focus on EIA behaviors. In the third section, Monthly-hourly means, monthly zonal means TEC as well as two cases of super-fountain effect are presented. Finally, we compare our results of this study with other results, discus about them and some probable future works are introduced.

## 2 Data and Methods

The international GNSS service (IGS) supplied TEC data with the time resolution of 2 hours determined from more than 400 IGS stations on a global scale. These TEC data can be used to study various phenomena in the ionosphere with diversity spatiotemporal distribution because of appropriate resolution with global coverage. TEC resolutions are 5° in longitude and 2.5° in latitude, 12 times every day. Longitude ranges from -180° to 180° degrees that includes 73 points with the resolution of 5°. Latitude ranges from -87.5° to 87.5° degrees that contain 71 points with the resolution of 2.5°. Because of high number of stations, good data quality and high precision are of characteristics of IONEX data. TEC is the column density of electrons measured in TEC units (TECU), in that 1TECU = $10^{16}$ electrons/$m^2$.

In this study, we used 19-year IONEX data in the period 1999 –2017 for both 23 and 24 solar cycles. IONEX data was downloaded from the below address: ftp://cddis.gsfc.nasa.gov/gnss/products/ionex.

This format stores the pseudo ranges and carrier phases (L1 and L2) for each satellite. A dual-frequency GPS receiver measures the difference in ionosphere delay between the L1 and L2 signals. The ionosphere TEC can be derived from delay between the L1 and L2 signal as below:

https://doi.org/10.5194/angeo-2021-34
Preprint. Discussion started: 23 June 2021

Annales Geophysicae Discussions

$$TEC = \frac{1}{40.3}\left[\frac{f_1^2 f_2^2}{f_1^2 - f_2^2}\right](P_2 - P_1) \quad (1)$$

where $f_1$ and $f_2$ are the corresponding high and low GPS frequency respectively and $P_1$ and $P_2$ are the group path lengths. The global ionosphere gridded data with the abovementioned time and spatial resolution can be provided from station data by CODE. CODE, which stands for the Centre for Orbit Determination in Europe, is one of seven analysis centers of IGS. TEC data of global grids is reconstructed by fitting the vertical TEC of IGS stations with the spherical harmonics function as below (*Guo et al.*, 2015):

$$TEC(\phi,\lambda) = \sum_{n=0}^{n_{\max}} \sum_{m=0}^{m_{\max}} P_{nm}(\phi)\left[\alpha_{nm}\cos(m\lambda) + \beta_{nm}\sin(m\lambda)\right], \quad (2)$$

where $\phi$ and $\lambda$ are the latitude and longitude respectively, $n_{\max}$ is the highest degree, $P_{nm}(\phi)$ is the normalized associated Legendre function, $a_{nm}$ and $\beta_{mn}$ are the spherical harmonics coefficients, and $n$ and $m$ are degree and order, respectively.

With the use of TEC data, statistical analyses were done in the following steps. At first, data decomposition was carried out in order to access various hourly, monthly and SA conditions. Zonal means of data were calculated (summation in all longitude for every latitude) for every abovementioned data decomposition. Monthly and annual means were calculated from zonal mean daily data. Hourly-monthly means of TEC were calculated in the same way. Hourly data were separated in each month, and then the calculation of hourly mean was conducted separately. We wrote some MATLAB scripts for reading IONEX data and doing all these calculations automatically.

Solar indices that are used to measure the amount of SA are sunspots (RZ), solar radio flux (F10.7cm) and magnetic activity indices like $A_p$ and $K_p$. The solar radio flux at 10.7cm (2800 MHz) is a convenient measure of solar spectral density that indicates solar cycles as well. Most of the F10.7 radio emissions originate from chromosphere and to some extent from corona of the solar's atmosphere. The F10.7 has been measured consistently in Canada since 1947, first in Ottawa, Ontario; and then at the Penticton Radio Observatory in British Columbia, Canada (http://lasp.colorado.edu/lisird/data/noaa_radio_flux). F10.7 is reported in terms of solar flux units (SFU). The F10.7 can vary from below 50 SFU to above 300 SFU, over the course of a solar cycle.

The classification of data into high and low SA was done based on monthly means of F10.7cm. Here we derived monthly means, annual means and total 19-year mean of F10.7 from daily data separately. With comparison of these means with 19-year mean of F10.7 (around 115 SFU), the monthly means whose values were greater that 19-yeay mean were classified into high SA, and vice versa into low SA. This type of classification of data is common in climate science.

## 3 Results

### 3-1 Climatology of EIA

https://doi.org/10.5194/angeo-2021-34
Preprint. Discussion started: 23 June 2021


In the solar cycle 23 that began in August 1996 and continued to December 2008, minimum annual average TEC was 14 TECU in 2008, and maximum annual average TEC was about 57 TECU in 2000 and 2002. In the current solar cycle, solar cycle 24, minimum annual average TEC was 14 TECU in 2009 and maximum annual average was 44 TECU in 2014. In June, July and August, maximum TEC is located in Northern Hemisphere (NH). The maximum of monthly mean TEC occurs in March, April and October (equinoxes), and the minimum of monthly mean TEC occurs in June, July and August (NH's summer solstice).

Figure 1 shows the hourly-monthly global distribution of TEC with 2-hour time spacing. Here for briefness of results, only hourly-monthly means of solstices are presented. The location of EIA crest increase from sunrise to afternoon and then fall again. The behavior of the EIA crest is mainly organized by the strength of the equatorial zonal electric field and Sun-Earth geometry, so EIA is presented by hourly-monthly and monthly means of IONEX data. Figure 1 shows the hourly-monthly global distribution of TEC with 2-hour time spacing. Here for briefness of results, only hourly-monthly means of solstices are presented. The maximum of hourly-monthly TEC is located in the lower latitudes and the minimum of hourly-monthly TEC is observed in winter hemisphere higher latitudes. The highest yellowish TEC distribution in low-latitude areas with two crests around the equator that moves westward against the primary eastwards Pedersen current is EIA. The maximum of hourly-monthly mean TEC is around 55 TECU in June, while the maximum of hourly-monthly mean TEC in July is 45 TECU. The maximum of hourly-monthly mean TEC is around 70 TECU in December, while the maximum of hourly-monthly mean TEC in January is 55 TECU.

There is some latitude oscillation of the EIA during its longitudinal westward displacement due to summer to winter neutral wind. The lowest bluish TEC distributions in high-latitude areas in Arctic region do not receive any solar radiation (figure 1). The low values of TEC from Arctic bow equatorward and form a low-value of TEC in mid-latitude in front of the crests which is similar to the daily quiet variation ($S_q$).

Asymmetry between two crests of the equatorial anomaly due to interaction of interhemispheric wind and fountain effect can be interpreted in the following ways. In NH summer, the summer-to winter wind brings the plasma upward and equatorward, whereas the fountain effect tends to diffuse the plasma to downward and poleward direction (*Mo et al.*, 2018). As seen in fig1. the electron density accumulates at location closer to the equator which show the dominance effect of neutral wind in the morning (between 04 to 12 UTC). But after 14 UTC the northern EIA crest forms in poleward location with more plasma pile up there because of dominance of fountain effect. After 18 to 20 UTC the southern crest disappear similar to satellite observations of *Mo et al.* (2018). Bowing of crest towards southern hemisphere (SH) at 16 to 20 UTC also compatible with neutral wind effects. In the SH in winter solstice, a downward diffusion produced by the fountain effect has the same direction as that produced by the summer-to-winter wind, which is compatible with stronger EIA crest of SH between 06 to 08 UTC. This result is also compatible with *Tsai et al.* (2001).

https://doi.org/10.5194/angeo-2021-34
Preprint. Discussion started: 23 June 2021

Annales Geophysicae Discussions
Open Access

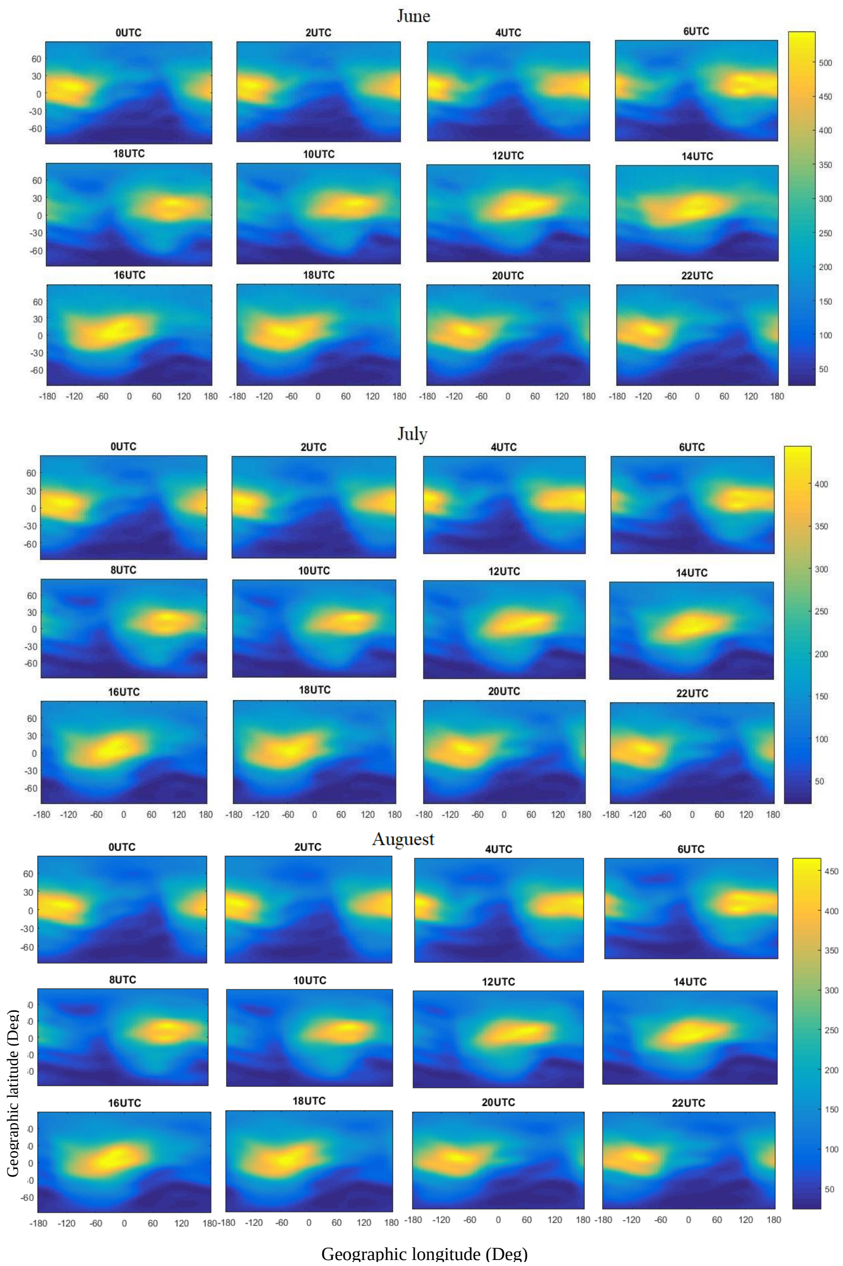


**Figure 1.** Hourly-monthly means of global GNSS TEC (0.1 TECU) for NH summer (JJA) between 1999-2017. Top panel June, middle panel July and lower panel August from 00 to 22UTC.

https://doi.org/10.5194/angeo-2021-34
Preprint. Discussion started: 23 June 2021

Annales Geophysicae
Discussions
Open Access

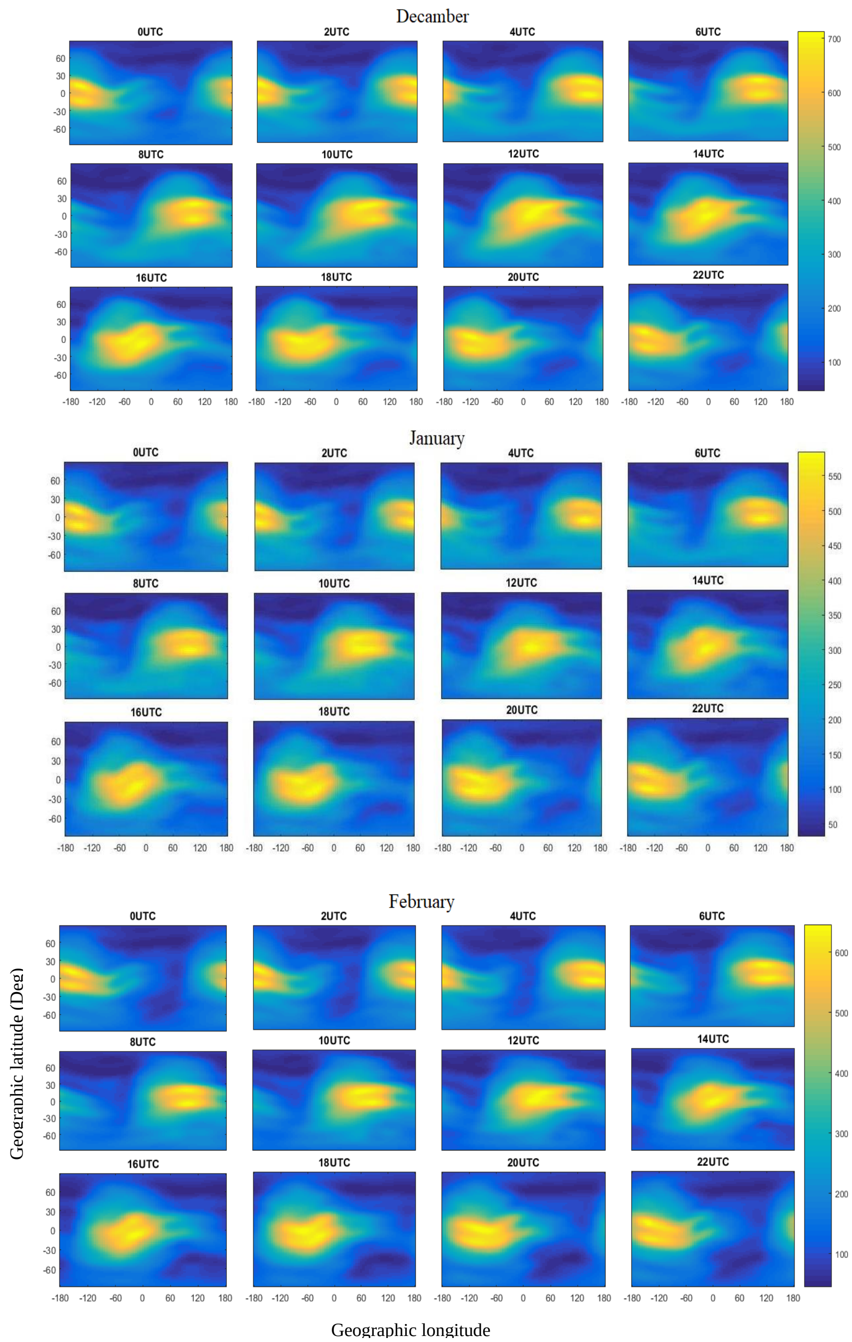


**Figure 2.** As Figure 1, but for NH winter (DJF). Top panel December, middle panel January and lower panel February.

https://doi.org/10.5194/angeo-2021-34
Preprint. Discussion started: 23 June 2021

Annales Geophysicae Discussions Open Access EGU

In NH winter, the summer to winter wind brings the plasma upward and poleward, and the fountain effect tends to diffuse the plasma to the same direction. As seen in fig2. between 06 to 18 UTC in SH the electron density pile up and the crest get strength due to sum up both neutral wind and fountain effects. But after 20 UTC the SH EIA crest get weaken and NH EIA developed and increased intensity compatible with *Mo et al.* (2018).

Table 1. Seasonal average of Maximum zonal-mean TEC between 1999-2017.

| Seasonal average | NH summer | NH spring | NH winter | NH fall |
|---|---|---|---|---|
| Maximum zonal-mean TEC average (0.1TECU) | 262.4 | 370.6 | 326.6 | 351.9 |
| Geographic latitude of Maximum zonal-mean TEC (deg) | 12.5 | 0.0 | -7.5 | -2.5 |

In figure 3, the monthly zonal means TEC for a period of 19 years were presented. As can be seen in the figure, the highest TEC is in March, April and October (northern hemisphere spring and autumn equinox), and the lowest is in June, July and August (NH summer solstice). These are compatible with the results of presented in Table 1. In addition, March's zonal mean TEC values are higher than September TEC value or TEC in NH spring equinox is higher than fall equinox. The result also can be seen in Table 1 is similar to results that was reported by *Meza et al.,* (2012). The pole that receives Sun's radiation has higher value of zonal mean TEC than that pole that dos not receives Sun's radiation. For example, in NH summer (June, July and August) zonal mean TEC is higher than that in SH's pole. Bimodal forms can be seen around the equator corresponding to EIA, which has a meridional shift in different months. These bimodal forms are pronounced after SA decomposition (see figure 4).

It is clear that maximum monthly mean TEC position and magnitude depends on summer to winter neutral wind and solar declination angle. Maximum zonal mean TEC is located in SH in December, January and February. Famous winter ionosphere anomaly can also be seen in figure 3 as well. As seen in Fig.3, semiannual variation of TEC can be better seen in the EIA oscillation due to the interaction of both effects of solar zenith angle and summer to winter neutral atmospheric circulation which result in changing amount of oxygen to nitrogen ratio. The resulting effect is increased EIA crest from January to May with maximum monthly zonal mean TEC in March (first row of Fig.3). Then decreased from May until August with minimum monthly zonal mean TEC of EIA in July (second row of Fig.3). Again monthly zonal mean TEC of EIA is increased from September to December with maximum monthly zonal mean in November (third row of Fig.3).

In NH summer, the summer to winter wind brings the plasma upward and equatorward, whereas the fountain effect tends to diffuse the plasma to downward and poleward direction. So,

https://doi.org/10.5194/angeo-2021-34
Preprint. Discussion started: 23 June 2021



one can see the both effects of the fountain effect and solar zenith angle in monthly zonal mean TEC and EIA crest. On the other hand, the neutral wind effect in monthly mean TEC may be suppressed by fountain effect and solar zenith angle dominate on equatorial magnetic effects.

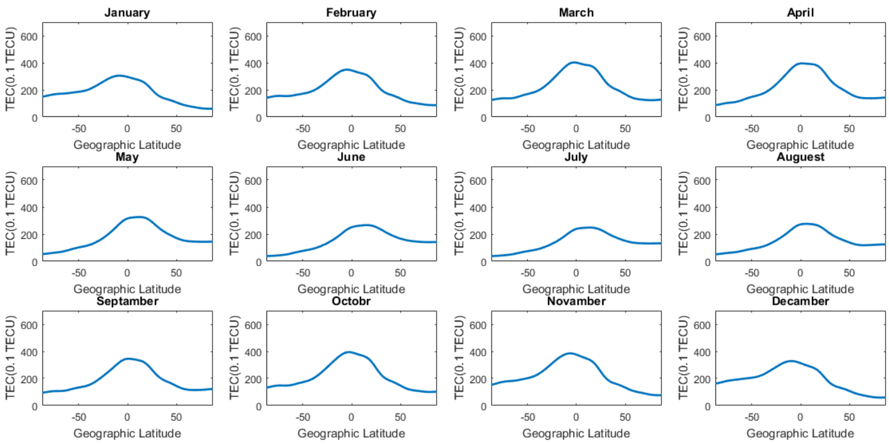


**Figure 3.** Zonal mean of the monthly means TEC (0.1 TECU) from January to December 1999-2017 of GNSS data.

After decomposing monthly data in terms of SA, the monthly zonal means TEC (0.1 TECU) is presented in figure 4. So low and high before name of a month indicates monthly mean TEC of that month in low and high SA condition. As seen in figure 4, the EIA greatly changes in different SA, especially in equinoxes. The steepness of zonal mean TEC with respect to latitude ($\frac{\partial TEC_{zonal\,mean}}{\partial y}$) is greater in equinoxes than solstices and in high SA than low SA. The bimodal forms around the equator corresponding to EIA are clearer in zonal mean TEC of high SA than low SA. There are some fluctuations on zonal mean TEC in mid-latitude (around 40°-50°) due to upward planetary wave (PW) propagation that is more pronounced in equinox and in low SA. Same results have also been observed in sporadic E layer ($E_s$) of Tehran region (*Karami et al.*, 2012). These fluctuations also exist in NH's winter, but isn't observed in NH's summer. This can explain by Charney-Drazin criteria in which stationary PW can't penetrate in the easterly and strong westerly winds of middle atmosphere (*Andrews et al.*, 1987*; Charney and Drazin*, 1961). According to this criteria vertical PW propagation is weaker in NH' s winter than equinoxes. Consequently, these mid-latitude fluctuations are more obvious at equinoxes than winter solstice when polar vortex is too strong. Upward stationary PWs propagation and their energy deposition at the critical layer of neutral atmosphere is projected in the ionospheric layer. According to wind shear theory, vertical wind shear associated with ion-neutral collision and Lorenz electromagnetic force result in ions convergence in lower ionosphere and consequently increase in TEC (*whitehead* 1961; *Karami et al.*, 2012). Another study demonstrated the competing influences of the vertical electric field and the zonal wind in the evening $E_s$ layer processes (*Abdu et al.*, 2003). As seen in figures 4a, 4b and 4d these mid-latitude fluctuations are obvious in winter, spring and fall, especially in NH with more stationary PW activities.

https://doi.org/10.5194/angeo-2021-34
Preprint. Discussion started: 23 June 2021

Annales Geophysicae
Discussions

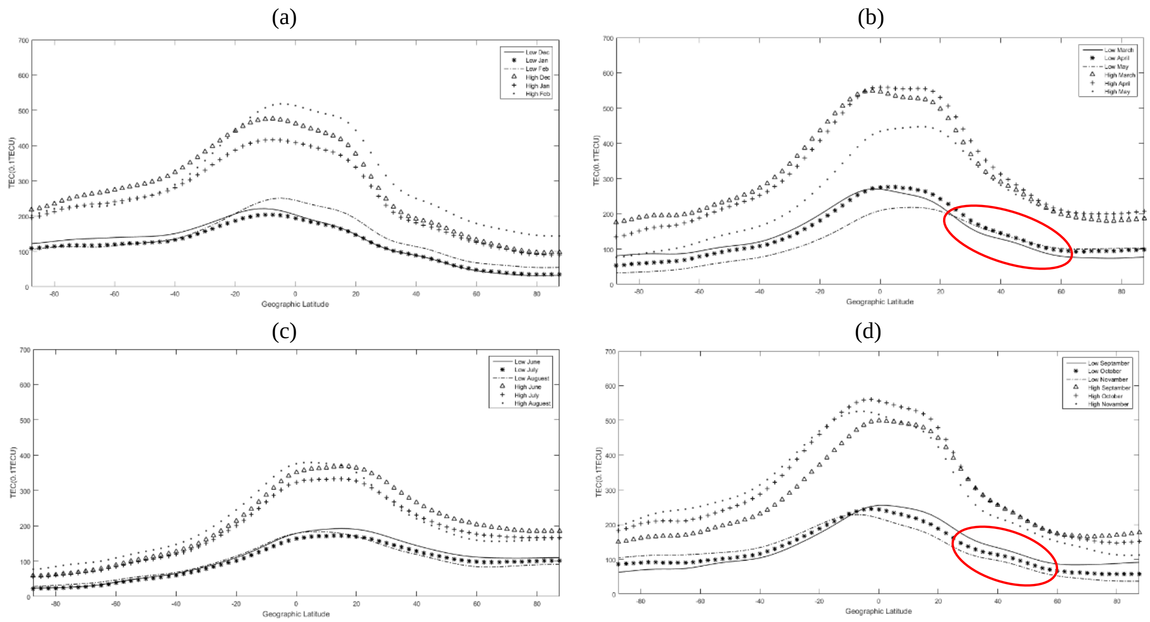


**Figure 4.** Monthly zonal mean TEC (0.1 TECU) a) DJF b) MAM c) JJA d) SON 1999-2017 of GNSS data in different high and low SA. Red circles represent mid-latitude fluctuations due to PW activity.

According to the figure 4, in December, January and February, which is the NH winter, the values of TEC during high SA are greater than the mean values in SH winter. In NH spring, maximum of TEC is again higher than SH spring. These results would seem to show maximum values in low-latitude regions, which clarify EIA intensity, are produced by the modulation of PW activities by SA.

### 3-2 Super-fountain Effect on Zonal Mean TEC

During the magnetic solar storms, the magnitude of TEC increases greatly at mid-latitude, that is known as super-fountain effect. During these phenomena, low latitude plasmas lift to much higher altitudes across the horizontal magnetic field lines via E×B drift, then diffuse down the magnetic field lines on both sides of the equator due to gravity and plasma pressure gradient forces (*Anderson* 1973; *Horvath and Lovell*, 2008; *Lu et al.*, 2013; *Tsurutani et al.*, 2004). In order to detect super-fountain effect, we prepared 15-day zonal mean from a week before up to a week after two solar storms from maximum daily zonal TEC values. Then we calculated TEC disturbance with removing maximum daily zonal TEC from the prepared mean. To keep it short, 4-day of results are presented in figures 5 and 6. For example, we present here results of Halloween solar storm in 2003 and another storm in 20 January, 2005. Two TEC peaks associated with the EIA show a pronounced displacement from tropical regions to mid latitudes prior to the storm onset (see figures 5a and 5b). The magnitude of the TEC anomaly in NH middle latitudes reaches

https://doi.org/10.5194/angeo-2021-34
Preprint. Discussion started: 23 June 2021

Annales Geophysicae Discussions Open Access EGU

the surprising value of 120 TECU during this storm (see figure 5c). Another super-fountain effect associated with solar storm in 20 January, 2005 is not as strong as Halloween and maximum TEC anomaly reaches the value of around 25 TECU in NH. Interhemispheric wind from summer hemisphere to winter hemisphere probably result in asymmetry in super-fountain effect. As the magnitude of zonal mean TEC increases greatly at middle latitudes, its magnitude decreases near the equatorial regions due to the consistency by plasma redistribution (see figures 5c and 6d). Even though the super-fountain effect is necessary for increasing of TEC at middle latitudes, its effect can induce subauroral disturbance electric fields to high latitudes (*Foster and Rideout*, 2005). This high latitude anomaly can be seen in figures 6a and 6d especially in SH.

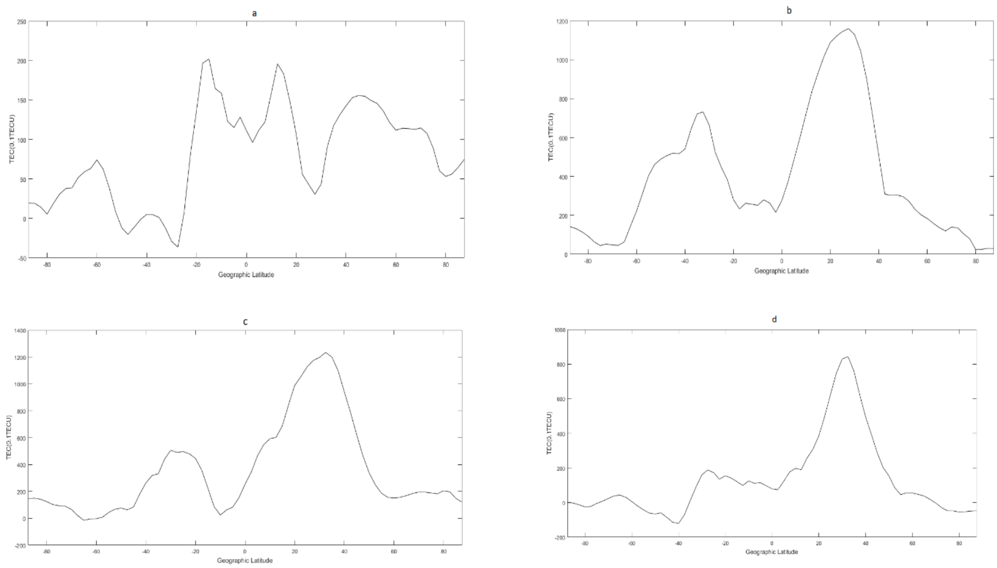


**Figure 5.** Super-fountain effect on zonal mean TEC (0.1 TECU) during solar storm (Halloween solar storm) a) 28 October, b) 29 October c) 30 October and d) 31 October 2003.

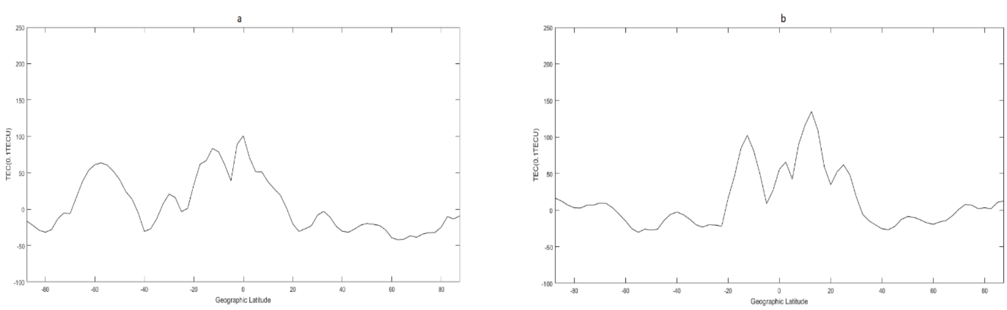

https://doi.org/10.5194/angeo-2021-34
Preprint. Discussion started: 23 June 2021



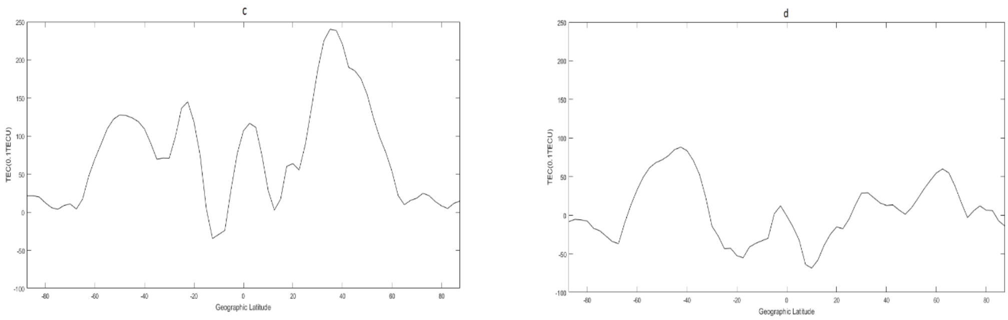


**Figure 6.** Super-fountain effect on zonal mean TEC (0.1 TECU) a) 19 January, b) 20 January c) 21 January and d) 22 January.

## 4 Conclusion

We used the global TEC from 1999 to 2017, during two recent solar cycles to study the climatological means TEC with spatiotemporal resolution of 5°×2.5° for every 2-hour IONEX data. Climatology zonal mean TEC reduced gradually from the tropical regions to high-latitude regions, and the maximum in tropical regions clearly displays EIA (compatible with (*Liu and Chen* 2009*; Mannucci et al.*, 1998; *Mazzella et al.*, 2017; *Parwani* 2019)). Monthly-hourly means of TEC, similar to another study, exhibited two plasma crests in tropical regions moving westward in longitude direction with different features (*Guo et al.*, 2015). In NH summer, the summer-to winter wind brings the plasma upward and equatorward, whereas the fountain effect tends to diffuse the plasma to downward and poleward direction (*Mo et al.*, 2018). The electron density accumulates at location closer to the equator which show the dominance effect of neutral wind in the morning (between 04 to 12 UTC). But after 14 UTC the northern EIA crest forms in poleward location with more plasma pile up there because of dominance of fountain effect. Zonal mean TEC frequently showed bimodal forms around the equator as EIA, which has different meridional maximum in different months.

Some fluctuations on zonal mean TEC in mid-latitude (around 40°-50°) due to upward stationary PW propagation was detected, which are pronounced in equinox and in low SA. These fluctuations also existed in NH winter, but wasn't observed in NH summer. The results are compatible with Charney-Drazin criteria (*Andrews et al.*, 1987; *Charney and Drazin* 1961), and also confirm previous findings about $E_s$ layer processes (*Abdu et al.*, 2003; *Karami et al.*, 2012).

Two cases of super-fountain effect during the magnetic solar storms were detected by anomaly from maximum zonal mean TEC. The peaks associated with the EIA were displaced from tropical regions to middle latitudes prior to the storm onset (see figures 5a and 5b). The magnitude of the TEC anomaly in Halloween solar storm reached the surprising value of 120 TECU.

Climatology values of TEC can be used for any other studies that intend to evaluate perturbation values. So many other case studies of lithosphere-atmosphere-ionosphere interactions, lower-upper atmosphere interaction and magnetosphere-ionosphere interactions can find their anomaly from these monthly means. Some other transient effects like traveling ionosphere disturbances can also be observed through these data. Higher statistical orders like correlation, covariance, standard division and etc. can be done in further studies as well.

**Acknowledgments**

We are very grateful to CODE of AIUB, Bern for providing TEC data and LISIRD for providing solar activity indices.

**Reference**

Abdu, M. A., J. W. MacDougall, I. S. Batista, J. H. A. Sobral, and P. T. Jayachandran (2003), Equatorial evening prereversal electric field enhancement and sporadic E layer disruption: A manifestation of E and F region coupling, *J. Geophys. Res.*, 108(A6), 1254, doi:10.1029/2002JA009285,

Appleton, E.V. (1946), Two anomalies in the ionosphere, *Nature*, 157, 691.

Andrews, D. G., J. R. Holton and C. B. Leovy (1987), Middle Atmosphere Dynamics, Academic press.

Charney, J. G., and P. G. Drazin (1961), Propagation of planetary scale disturbances from the lower into the upper atmosphere, *J. Geophys. Res*., 66, 83–109.

Chou, M. Y., C. C. H. Lin, J. Yue, H. F. Tsai, Y. Y. Sun, J. Y. Liu, and C. H. Chen (2017), Concentric traveling ionosphere disturbances triggered by Super Typhoon Meranti (2016), *Geophys. Res. Lett*., 44, 1219–1226, doi:10.1002/2016GL072205.

Codrescu, M. V., K. L. Beierle, T. J. Fuller-Rowell, S. E. Palo, and X. Zhang (2001), More total electron content climatology from TOPEX/Poseidon measurements, *Radio Sci.*, 36, 325-333.

Dashora, N., and S. Suresh (2015), Characteristics of low-latitude TEC during solar cycles 23 and 24 using global ionospheric maps (GIMs) over Indian sector, *J. Geophys. Res.*, 120, 5176–5193, doi:10.1002/2014JA020559.

Ducic, V., J. Artru, and P. Lognonné (2003), Ionospheric remote sensing of the Denali Earthquake Rayleigh surface waves. *Geophys. Res. Lett*. 30 (18), 1951. http://dx.doi.org/ 10.1029/2003GL017812.

Eyelade, V.A., A.O. Adewale, A.O. Akala, , O.S. Bolaji, and A.B. Rabiu (2017), Studying the variability in the diurnal and seasonal variations in GPS TEC over Nigeria. *Ann. Geophys*., 35, 701 – 710.

Fejer, B. G., J. W. Jensen and S. Y. Su (2008), Quiet time equatorial F region vertical plasma drift model derived from ROCSAT-1 observations, *J. Geophys. Res*., 113 (A5), http://dx.doi.org/10.1029/2007JA012801.

Foster, J. C., and W. Rideout (2005), Mid-latitude TEC enhancements during the October 2003 superstorm, *Geophys. Res. Lett*., 32, L12S04, doi:10.1029/2004GL021719.

Fuller-Rowell TJ. (1998), The “thermospheric spoon”: A mechanism for the semiannual density variation. *J. Geophys. Res*., 103: 3951–3956. doi: 10.1029/97JA03335.

https://doi.org/10.5194/angeo-2021-34
Preprint. Discussion started: 23 June 2021



Guha, A., B. Paul, M. Chakraborty, and B. K. De (2016), Tropical cyclone effects on the equatorial ionosphere: First result from the Indian sector, *J. Geophys. Res.*, 121, 5764–5777, doi:10.1002/2016JA022363.

Guo, J., et al. (2015), Temporal-Spatial Variation of Global GPS-Derived Total Electron Content, 1999-2013. *PLoS ONE*, vol. 10, no. 7. Gale OneFile: Health and Medicine, Accessed 28 Dec. 2019.

Gao, Y., and Z. Liu (2002), Precise Ionosphere Modeling Using Regional GPS Network Data. *Journal of Global Positioning Systems*. 1. 18-24. 10.5081/jgps.1.1.18.

Horvath, I. (2006), A total electron content space weather study of the nighttime Weddell Sea Anomaly of 1996/1997 southern summer with TOPEX/Poseidon radar altimetry, *J. Geophys. Res*., 111, A12317, doi:10.1029/2006JA011679.

Horvath, I., and B. C. Lovell (2008), Formation and evolution of the ionospheric plasma density shoulder and its relationship to the superfountain effects investigated during the 6 November 2001 great storm, *J. Geophys. Res*., 113, A12315, doi:10.1029/2008JA013153.

Huang, H., L. Liu, Y. Chen, H. Le, and W. Wan (2016), A global picture of ionospheric slab thickness derived from GIM TEC and COSMIC radio occultation observations, *J. Geophys. Res*., 121, 867–880, doi:10.1002/2015JA021964.

Jin, S. G., O. Occhipinti, and R. Jin (2015), GNSS ionospheric seismology: Recent observation evidences and characteristics, *Earth-Sci. Rev*., 147, 54–64, doi: 10.1016/j.earscirev.2015.05.003.

Jee, G., R. W. Schunk, and L. Scherliess (2004), Analysis of TEC data from the TOPEX/Poseidon mission, *J. Geophys. Res.*, 109, A01301, doi:10.1029/2003JA010058.

Karami, K., S. Ghader , A. A. Bidokhti, M. Joghataei, A. Neyestani, and A. Mohammadabadi (2012), Planetary and tidal wave-type oscillations in the ionospheric Sporadic-E layers over Tehran region, *J. Geophys. Res*., *117*, A04313, 6 PP, doi:10.1029/2011JA017466.

Kelley, M. C., M. N. Vlasov, J. C. Foster, and A. J. Coster (2004), A quantitative explanation for the phenomenon known as storm enhanced density, *Geophys. Res. Lett*., 31, L19809, doi:10.1029/ 2004GL020875.

Liao X. (2000), Carrier phase based ionosphere recovery over a regional area GPS network. M.Sc. Thesis, Univ. of Calgary, Canada.

Li Z. G., Z. Y. Cheng, C. G. Feng, W. C. Li, and H. R. Li (2007), A study of prediction models for ionosphere. *Chinese Journal of Geophysics*, 50, 327–337.

Lin, C. H., J. Y. Liu, T. W. Fang, P. Y. Chang, H. F. Tsai, C. H. Chen, and C. C. Hsiao (2007), Motions of the equatorial ionization anomaly crests imaged by FORMOSAT-3/ COSMIC, Geophys. Res. Lett., 34, L19101, doi:10.1029/ 2007GL030741.

Liu, L., W. Wan, B. Ning, and M. L. Zhang (2009), Climatology of the mean total electron content derived from GPS global ionospheric maps, *J. Geophys. Res*., 114, A06308, doi:10.1029/2009JA014244.

https://doi.org/10.5194/angeo-2021-34
Preprint. Discussion started: 23 June 2021




Meng Y, et al (2011), Spatial distribution of antarctic ionosphere TEC based on GPS. *Acta Geodaetica Cartogr Sin*., 40(1):37–40

Meza, A., M. P. Natali, and L. I. Fernández (2012), Analysis of the winter and semiannual ionospheric anomalies in 1999–2009 based on GPS global International GNSS Service maps, *J. Geophys. Res*., 117, A01319, doi:10.1029/2011JA016882.

Mo, X. H., Zhang, D. H., Liu, J., Hao, Y. Q., Ye, J. F., Qin, J. S., … Xiao, Z. (2018), Morphological characteristics of equatorial ionization anomaly crest over Nanning region. *Radio Science*, 53, 37–47. https://doi.org/10.1002/ 2017RS006386.

Mukhtarov, P., D. Pancheva, B. Andonov, and L. Pashova (2013), Global TEC maps based on GNSS data: 1. Empirical background TEC model, *J. Geophys. Res.,*118, doi:10.1002/jgra.50413.
Occhipinti, G., R. Lucie, L. Philippe, and W. Shingo (2013), From Sumatra 2004 to Tohoku-Oki 2011: the systematic GPS detection of the ionospheric signature induced by tsunamigenic earthquakes. *J. Geophys. Res.*, 118 (6), 3626–3636.

Saito, A., S. Fukao, and S. Miyazaki (1998), High resolution mapping of TEC perturbations with the GSI GPS network over Japan. *Geophysical Research Letters*.; 25, 3079–3082. doi: 10.1029/98GL52361.

Savastano, G., et al. (2017), Real-Time Detection of Tsunami Ionospheric Disturbances with a Stand-Alone GNSS Receiver: A Preliminary Feasibility Demonstration. *Sci Rep* 7, 46607 doi:10.1038/srep46607.

Schaer, S., G. Werner, and J. Feltens (1998), IONEX: The Ionosphere Map Exchange Format Version 1. Proceedings of the IGS Analysis Centers workshop, Darmstadt, Germany. February 9–11, 233–247.

Schunk, R. W., and A. F. Nagy (2000), Ionospheres, Cambridge Univ. Press, New York.

Stolle, C., Manoj, C., Lühr, H., Maus, S., & Alken, P. (2008), Estimating the daytime equatorial ionization anomaly strength from electric field proxies. *Journal of Geophysical Research*, 113, A09310. https://doi.org/10.1029/2007JA012781.
Tapping, K.F. (1987), Recent Solar Radio Astronomy at Centimeter Wavelengths: The Temporal Variability of the 10.7-cm Flux, *J. Geophys. Res*., 92(D1), 829-838.

Taranenko, Y. N., U. S. Inan, and T. F. Bell (1993), The interaction with the lower ionosphere of electromagnetic pulses from lightning: Heating, attachment, and ionization, *Geophys. Res. Lett., 20(15)*, 1539–1542.

Wu, C. C., Fry, C. D., Liu, J.-Y., Liou, K., & Tseng, C. L. (2004). Annual TEC variation in the equatorial anomaly region during the solar minimum: September 1996-August 1997. *Journal of Atmospheric and Solar: Terrestrial Physics*, 66, 199–207. https://doi.org/10.1016/ j.jastp.2003.09.017.